Journal of Power Sources 218 (2012) 106–112

Contents lists available at SciVerse ScienceDirect

Journal of Power Sources

journal homepage: www.elsevier.com/locate/jpowsour

The phase stability and electrical conductivity of Bi_2O_3 ceramics stabilized by Co-dopants

Sea-Fue Wang*, Yung-Fu Hsu, Wen-Chiao Tsai, Hsi-Chuan Lu

Department of Materials and Mineral Resources Engineering, National Taipei University of Technology, 1, Sec. 3, Chung-Hsiao E. Road, Taipei 106, Taiwan, ROC

HIGHLIGHTS

- All $Bi_{0.76}Y_{0.24-x}M_xO_{1.5+\delta}$ reported a lower sintering temperature than $Bi_{0.76}Y_{0.24}O_{1.5}$.
- Lattice constant of $Bi_{0.76}Y_{0.24}O_{1.5}$ rose with dopants of Gd^{3+}, Sc^{3+}, or Zr^{4+}, but not Nb^{5+}.
- $Bi_{0.76}Y_{0.20}Zr_{0.04}O_{1.5+\delta}$ ceramic has the electrical conductivity of 0.55 S cm^{-1} at 700 °C.
- Co-doped Bi_2O_3 ceramics have greater conductivities than single-dopant counterparts.
- The larger conductivity may be triggered by the larger lattice constants.

ARTICLE INFO

Article history:
Received 25 March 2012
Received in revised form
12 June 2012
Accepted 13 June 2012
Available online 20 June 2012

Keywords:
Solid oxide fuel cell
Electrolyte
Bismuth oxide
Electrical conductivity

ABSTRACT

In this study, Gd_2O_3, Nb_2O_5, Sc_2O_3, ZrO_2, and BaO are chosen as co-dopants with Y_2O_3 to stabilize δ phase Bi_2O_3 ceramics. Under a fixed dopant concentration, the effects of the co-dopants on the phase stability and electrical properties of $Bi_{0.76}Y_{0.24-x}M_xO_{1.5+\delta}$ (M = Gd, Nb, Sc, Zr, and Ba) are investigated. Based on the study results, all co-doped specimens exhibit a sintering temperature lower than that of the $Bi_{0.76}Y_{0.24}O_{1.5}$ ceramic. The $Bi_{0.76}Y_{0.24-x}Gd_xO_{1.5}$, $Bi_{0.76}Y_{0.24-x}Nb_xO_{1.5+\delta}$, and $Bi_{0.76}Y_{0.24-x}Sc_xO_{1.5}$ ceramics retain a cubic fluorite structure of δ-Bi_2O_3 phase while $Bi_{0.76}Y_{0.24-x}Ba_xO_{1.5-\delta}$ displays a mixture of cubic and rhombohedral phases. Despite the fact that the ionic radius of Sc^{3+} and Zr^{4+} ions are smaller than that of Y^{3+} ion, the lattice constant of the $Bi_{0.76}Y_{0.24}O_{1.5}$ ceramic rises with the Gd_2O_3, Sc_2O_3, or ZrO_2 replacement but drops with the Nb_2O_5 substitution. Of the compositions studied, the $Bi_{0.76}Y_{0.20}Zr_{0.04}O_{1.5+\delta}$ ceramic emerges with the best electrical conductivities of 0.27 and 0.55 Scm^{-1} at 600 and 700 °C, much higher than those of the Y_2O_3-doped and ZrO_2-doped Bi_2O_3 ceramics. It is observed that, with the same total dopant concentration, the co-dopant stabilized Bi_2O_3 ceramics outperforms their single-dopant stabilized counterparts in terms of conductivity, probably due to the larger lattice constants.

1. Introduction

In recent years, development of intermediate-temperature solid oxide fuel cells (IT-SOFCs) operating at temperatures between 500 and 700 °C has solicited increasing attention due to major competitive advantages like cost effectiveness, ease of materials selection, and improved long term stability [1,2]. In the field of IT-SOFC research and development, considerable efforts have been invested to improve the ionic conductivity of electrolytes and reduce the polarization resistance (R_P) of electrodes [3]. Of several electrolyte candidates, face-centered cubic (fcc) δ-Bi_2O_3 is recognized as one of the most important oxide ionic conductors [4,5]. The δ phase, one of the six polymorphs (α, β, γ, δ, ε, and ω) [6], exists only in temperatures ranging from 730 to 824 °C (its melting point) and transforms into the monoclinic phase on cooling below 630 °C. Large thermal hysteresis is usually observed when the δ phase undergoes cooling, and one of the two intermediate metastable phases – the tetragonal β phase or the body-centered cubic (bcc) γ phase – may be formed respectively at 650 °C or 639 °C. These intermediate metastable phases usually transform into α-Bi_2O_3 on further cooling [7–9]. The electrical conductivity of the high temperature δ-Bi_2O_3 phase displays a magnitude one to two orders higher than those of stabilized zirconia at compatible temperatures [8,10,11], due to the ability of Bi^{3+} to accommodate the highly disordered surroundings and the fact that pure δ-Bi_2O_3 is marked with a large number of oxygen vacancies and a high anion mobility caused by the high polarizability of Bi^{3+} with its lone-pair $6s^2$ electrons [12].

* Corresponding author. Tel.: +886 2 2771 2171x2735; fax: +886 2 2731 7185.
E-mail addresses: seafuewang@yahoo.com, sfwang@ntut.edu.tw (S.-F. Wang).

0378-7753/$ – see front matter © 2012 Elsevier B.V. All rights reserved.
http://dx.doi.org/10.1016/j.jpowsour.2012.06.056

The high temperature form of δ-Bi_2O_3 can be retained at ambient temperature by substituting the Bi^{3+} position with isovalent or aliovalent cations such as M_2O_3 (M: La, Y, Fe, Sb, and rare earth element) [6,13–21], M_2O_5 (M: Ta, Nb, Sb, and V) [15,22,23], MO_2 (M: Zr, Sn, Te, Ti, and W) [24,25], and MO (M: Ca, Sr, Ba, and Pb) oxides [6,16]. It was reported that dopants with an ionic radius smaller than that of Bi^{3+} helped stabilize the high temperature δ-phase due to the induced contraction of the open structure of δ-Bi_2O_3 [26]. On the other hand, introduction of dopants with a relatively large ionic radius like La, Nd, Sm, and Gd into the Bi_2O_3 lattice was found to induce the formation of a rhombohedral structure in Bi_2O_3 (also a highly conductive phase) [8]. Such substitutions to stabilize the δ phase generally result in lowering the ionic conductivity of δ-Bi_2O_3 since the differences in ionic radius between Bi^{3+} and the doping cations induce lattice distortion. Usually, maintaining a lower dopant concentration while retaining the δ-phase leads to a higher ionic conductivity [18].

Compared to single-dopant systems, co-doping using two different metal oxides facilitates the stabilization of the δ-Bi_2O_3 down to room temperature at a lower doping concentration [27,28] due to the entropy increase in the quaternary systems. Several studies have been conducted recently to examine the effects of co-dopants, including Y–Ln (Ln = Er, Gd, Sm, Pr, Nb, Zr), Te–Ln (ln = La, Sm, Gd, Er), Ca–W, Dy–W, Nb–Ho, and Er–Nb oxides [14,26,28–32], on the stabilization of δ-Bi_2O_3 and the resulting electrical conductivity. While growth in conductivity was noted in few compositions, the effect of co-doping on the conductivity of δ-Bi_2O_3 remains inconclusive; further investigations are therefore needed. In this study, Y_2O_3 combined with oxide-containing cations in various ionic radii and valence numbers, including Gd_2O_3, Nb_2O_5, Sc_2O_3, ZrO_2, and BaO, were used as co-dopants to stabilize the δ phase Bi_2O_3. The effects of the co-dopants on the phase stability and electrical properties of $Bi_{0.76}Y_{0.24-x}M_xO_{1.5+\delta}$ (M = Gd, Nb, Sc, Zr, and Ba) were investigated and discussed.

2. Experimental procedure

Powders of the Bi_2O_3-based electrolyte materials used in this investigation were synthesized by a solid state reaction method. High-purity Bi_2O_3 (SHOWA, Reagent grade), Y_2O_3 (ALFA AESAR, Reagent grade), Gd_2O_3 (SHOWA, Reagent grade), Nb_2O_5 (SHOWA, Reagent grade), Sc_2O_3 (STREM CHEMICALS, Reagent grade), ZrO_2 (ACROS, Reagent grade), and $BaCO_3$ (JCI, Reagent grade) were used as raw materials. Bi_2O_3-based oxides based on the constituents of $Bi_{0.76}Y_{0.24-x}M_xO_{1.5+\delta}$ (M = Gd, Nb, Sc, Zr, and Ba; $x = 0.02, 0.04, 0.06, 0.08$, and 0.10) were mixed and milled in methyl alcohol solution using polyethylene jars and zirconia balls for 24 h and then oven-dried at 80 °C overnight. After drying, the powders were calcined at temperatures ranging from 775 °C to 825 °C for 2 h at a heating rate of 5 °C min^{-1}, re-milled in methyl alcohol for 24 h, and oven-dried at 80 °C overnight. X-ray diffraction (XRD, Simens D5000) was used for phase identification on the calcined powders. For electrical conductivity measurement, the powders were added with a 5 wt% of 15%-PVA solution and pressed into disc-shaped compacts under a uniaxial pressure of 0.9 tons cm^{-2}. The samples were then heat treated at 550 °C for 4 h to eliminate the PVA and sintered at 825–1050 °C for various durations (heating rate = 5 °C min^{-1}). The liquid displacement method was adopted to measure the densities of the specimens while conductivity as a function of temperature was measured by a standard four-probe method in air using Keithley 2400 at temperatures ranging from 25 to 800 °C at a heating rate of 2 °C min^{-1}. Scanning electron microscopy (SEM, Hitachi S4700) studies on the fracture surfaces of the sintered discs were performed for microstructure examination.

3. Results and discussion

In this study, $Bi_{0.76}Y_{0.24}O_{1.5}$ was used as the host material to evaluate the effects of co-doping on phase stability and electrical properties, due to the facts that this composition is located in the stable single-phase region of the Bi_2O_3–Y_2O_3 phase diagram [33] and marked with an electrical conductivity close to the highest in the Bi_2O_3–Y_2O_3 system as reported by Takahashi et al. [10,23]. Various ions, including Ba^{2+} (1.42 Å), Sc^{3+} (0.87 Å), Gd^{3+} (1.05 Å), Zr^{4+} (0.84 Å), and Nb^{5+} (0.74 Å), were selected to co-dope with Y^{3+} in the Bi_2O_3 lattice. The total doping concentration in Bi_2O_3 was maintained at 24 mol% and the co-dopants were formulated to replace the Y^{3+} ions in the Bi_2O_3 matrix, i.e. $Bi_{0.76}Y_{0.24-x}M_xO_{1.5+\delta}$ ($x = 0.0, 0.02, 0.04, 0.06, 0.08$, and 0.10). Under a fixed total dopant concentration, the effect of the ions co-doped with Y^{3+} on the characteristics of Bi_2O_3 were investigated since conductivity is known to depend on total dopant concentration and a higher dopant content generally results in a lower oxide ionic conductivity [8,18].

In the study, the host material of $Bi_{0.76}Y_{0.24}O_{1.5}$ was sintered at temperatures ranging from 950 to 1150 °C for 2 h and the maximum densification achieved at 1025 °C was 96% of the theoretical density (TD). As Fig. 1(a) reveals, the diffraction peaks of the XRD pattern were indexed to a cubic fluorite structure of δ- Bi_2O_3 phase (JCPDS card No. 84-1450). Its lattice constant was calculated to be 5.4940 Å, in accord with the results (5.493 Å) reported in the literature [21,34] but smaller than that of δ- Bi_2O_3 (0.56595 Å) [9] due to the difference in the ionic radius between Y^{3+} (1.02 Å) and Bi^{3+} (1.17 Å) (Fig. 2). At 500, 600, 700, and 800°C, the measured electrical conductivities of the densified $Bi_{0.76}Y_{0.24}O_{1.5}$ ceramic were respectively 0.01, 0.08, 0.26, and 0.56 Scm^{-1} (Fig. 4(a)), slightly higher than the results reported by Takahashi et al. [10]. Part of the Y^{3+} ions in the $Bi_{0.76}Y_{0.24}O_{1.5}$ host material was then replaced by various amounts of Ba^{2+}, Sc^{3+}, Gd^{3+}, Zr^{4+}, and Nb^{5+} ions.

Results of the sintering study on the $Bi_{0.76}Y_{0.24-x}M_xO_{1.5}$ ceramics indicated that all the co-doped specimens ($Bi_{0.76}Y_{0.24-x}Gd_xO_{1.5}$, $Bi_{0.76}Y_{0.24-x}Nb_xO_{1.5+\delta}$, $Bi_{0.76}Y_{0.24-x}Sc_xO_{1.5}$, $Bi_{0.76}Y_{0.24-x}Zr_xO_{1.5+\delta}$, and $Bi_{0.76}Y_{0.24-x}Ba_xO_{1.5-\delta}$ ceramics) showed a sintering temperature lower than that of the $Bi_{0.76}Y_{0.24}O_{1.5}$ ceramic. Achieving a sintered density greater than 95% TD, the $Bi_{0.76}Y_{0.24-x}Gd_xO_{1.5}$, $Bi_{0.76}Y_{0.24-x}Sc_xO_{1.5}$, and $Bi_{0.76}Y_{0.24-x}Zr_xO_{1.5+\delta}$ ceramics were densified at 950 °C and the $Bi_{0.76}Y_{0.24-x}Nb_xO_{1.5+\delta}$ ceramic at 975 °C. With sintering temperatures significantly lower than those of other systems, the $Bi_{0.76}Y_{0.24-x}Ba_xO_{1.5-\delta}$ ceramics could be densified at a temperature as low as 825 °C, indicating that the substitution of Ba^{2+} effectively reduced the sintering temperature of the $Bi_{0.76}Y_{0.24}O_{1.5}$ ceramic. It should be noted that, in the $Bi_{0.76}Y_{0.24-x}Sc_xO_{1.5}$ system, densification was obviously improved with the increase in the Sc^{3+} content; for instance, the sintered density rose from 96.1% TD for the $Bi_{0.76}Y_{0.22}Sc_{0.02}O_{1.5}$ ceramic to nearly 100% TD for the $Bi_{0.76}Y_{0.14}Sc_{0.10}O_{1.5}$ ceramic.

Fig. 1(b)–(f) presents the XRD patterns of the $Bi_{0.76}Y_{0.24-x}M_xO_{1.5}$ ceramics with the maximum densification and Table 1 lists the identified phase for each system. Similar to the $Bi_{0.76}Y_{0.24}O_{1.5}$ ceramics illustrated in Fig. 1(a), the $Bi_{0.76}Y_{0.24-x}Gd_xO_{1.5}$, $Bi_{0.76}Y_{0.24-x}Nb_xO_{1.5+\delta}$, and $Bi_{0.76}Y_{0.24-x}Sc_xO_{1.5}$ ceramics showed a cubic fluorite structure of δ-Bi_2O_3 phase regardless of the x values studied. No other second phase was visible in the XRD patterns. As reported in the literature, $Bi_{1-x}Gd_xO_{1.5}$ obtained a rhombohedral single phase with the x value ranging from 0.1 to 0.3 and a fcc phase at x of 0.35. $Bi_{1-x}Nb_xO_{1.5+\delta}$ obtained a pure fcc phase as the x value reached 0.15 [10,23]. It should be noted that Sc_2O_3, an effective dopant for stabilizing the cubic phase and thus increasing the ionic conductivity of ZrO_2, has not been used in the Bi_2O_3 system yet. Nevertheless, it is apparent in the present study that the

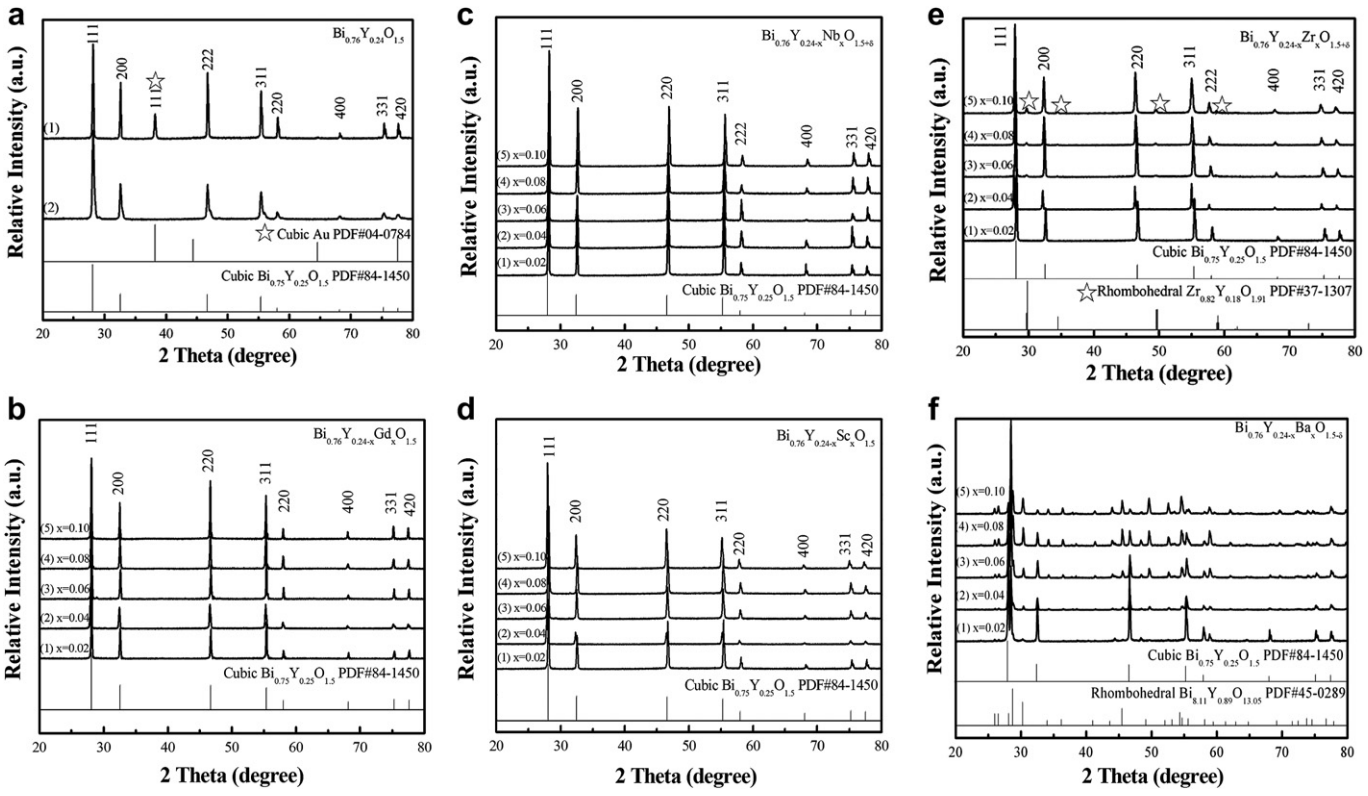

Fig. 1. XRD patterns of (a) $Bi_{0.76}Y_{0.24}O_{1.5}$ ceramic (1025 °C/2 h), (b) $Bi_{0.76}Y_{0.24-x}Gd_xO_{1.5}$ ceramic (950 °C/2 h), (c) $Bi_{0.76}Y_{0.24-x}Nb_xO_{1.5+\delta}$ ceramic (975 °C/2 h), (d) $Bi_{0.76}Y_{0.24-x}Sc_xO_{1.5}$ ceramic (950 °C/2 h), (e) $Bi_{0.76}Y_{0.24-x}Zr_xO_{1.5+\delta}$ ceramics (950 °C/2 h), and (f) $Bi_{0.76}Y_{0.24-x}Ba_xO_{1.5-\delta}$ ceramic (825 °C/2 h).

$Bi_{0.76}Y_{0.24-x}Gd_xO_{1.5}$, $Bi_{0.76}Y_{0.24-x}Nb_xO_{1.5+\delta}$, and $Bi_{0.76}Y_{0.24-x}Sc_xO_{1.5}$ systems with the concentration of co-dopant and Y^{3+} (i.e. Gd^{3+}/Y^{3+}, Nb^{5+}/Y^{3+}, and Sc^{3+}/Y^{3+}) set at the ratios of 22/2, 20/4, 18/6, 16/8, and 14/10 showed no sign of destabilizing the δ-Bi_2O_3 phase. The finding supported indirectly the observation that, with two dopants, the cubic phase of Bi_2O_3 could be stabilized with a lower total dopant concentration as compared to a single dopant system [26,27]. As revealed in Fig. 2, the calculated lattice constants of the $Bi_{0.76}Y_{0.24-x}Nb_xO_{1.5+\delta}$ ceramics gradually went down from 5.4906 to 5.4815 Å as the x value escalated from 0.02 to 0.10, caused by the smaller ionic radius of Nb^{5+} (0.74 Å) as compared to that of Y^{3+} (1.02 Å). The lattice parameter appeared to stay constant as the x value reached 0.6 and above, suggesting the possible formation of a second phase, which, however, was not observable in the XRD pattern due to its small quantity. For the $Bi_{0.76}Y_{0.24-x}Gd_xO_{1.5}$ and $Bi_{0.76}Y_{0.24-x}Sc_xO_{1.5}$ ceramics, the lattice constants increased slightly and almost linearly with the addition of Gd_2O_3 or Sc_2O_3, rising from 5.4919 to 5.5098 Å for the $Bi_{0.76}Y_{0.24-x}Gd_xO_{1.5}$ ceramic and from 5.4919 to 5.5098 Å for the $Bi_{0.76}Y_{0.24-x}Sc_xO_{1.5}$ ceramic. The ionic radius of Gd^{3+} ion (1.05 Å) is slightly larger and the ionic radius of Sc^{3+} ion (0.87 Å) smaller than that of Y^{3+} ion (Å). The exact reason for the smaller Sc^{3+} to trigger a slight lattice expansion in the $Bi_{0.76}Y_{0.24-x}Sc_xO_{1.5}$ ceramics is still unclear. However, two possibilities have been cited. One reason is the reduction of Sc^{3+} to Sc^{2+} associated with the creation of oxygen vacancies when substituted in the Bi^{3+} sites [17]. Or it might be due to a similar behavior observed by Jung et al.: double doping results in a considerably larger lattice parameter than is obtained from either of the dopants when they are singularly doped [26], since occupation in the interstitial sites is quite improbable in bismuth oxide lattice [31]. As indicated in Fig. 1(e), for the $Bi_{0.76}Y_{0.24-x}Zr_xO_{1.5+\delta}$ system, formation of the δ-Bi_2O_3 phase associated with the presence of a second $Zr_{0.82}Y_{0.25}O_{1.91}O_{1.5+\delta}$ phase was observed after sintering at 950 °C for 2 h, particularly with $x \geq 0.06$. The intensity of the peaks corresponding to the $Zr_{0.82}Y_{0.25}O_{1.91}$ compound rose as the content of ZrO_2 dopant in $Bi_{0.76}Y_{0.24-x}Zr_xO_{1.5+\delta}$ moved up. The lattic constant of the $Bi_{0.76}Y_{0.24-x}Zr_xO_{1.5+\delta}$ ceramics, as indicated by Fig. 2, significantly increased with the growth in the ZrO_2 content from 5.4932 to 5.5289 Å as the x value escalated from 0.02 to 0.10. Though the ionic radius of Zr^{4+} is smaller as compared to that of Y^{3+}, the formation of $Zr_{0.82}Y_{0.25}O_{1.91}$ consumed the Y_2O_3 content in the Bi_2O_3 matrix and

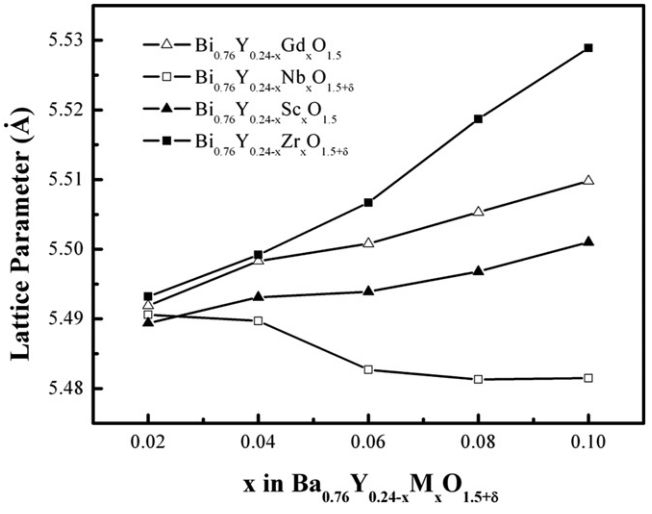

Fig. 2. Lattice constants calculated from the XRD patterns of the sintered $Bi_{0.76}Y_{0.24-x}M_xO_{1.5+\delta}$ ceramics.

Table 1
Crystal phases observed in the sintered $Bi_{0.76}Y_{0.24-x}M_xO_{1.5}$ (M = Gd, Nb, Sc, Zr, Ba) specimens.

Formulation			Sintering temperature	Phase present
$Bi_{0.76}Y_{0.24}O_{1.5}$			1025 °C/2 h	Cubic
$Bi_{0.76}Y_{0.24-x}Gd_xO_{1.5}$	$x = 0.02$	$Bi_{0.76}Y_{0.22}Gd_{0.02}O_{1.5}$	950 °C/2 h	Cubic
	$x = 0.04$	$Bi_{0.76}Y_{0.20}Gd_{0.04}O_{1.5}$	950 °C/2 h	Cubic
	$x = 0.06$	$Bi_{0.76}Y_{0.18}Gd_{0.06}O_{1.5}$	950 °C/2 h	Cubic
	$x = 0.08$	$Bi_{0.76}Y_{0.16}Gd_{0.08}O_{1.5}$	950 °C/2 h	Cubic
	$x = 0.10$	$Bi_{0.76}Y_{0.14}Gd_{0.10}O_{1.5}$	950 °C/2 h	Cubic
$Bi_{0.76}Y_{0.24-x}Nb_xO_{1.5+\delta}$	$x = 0.02$	$Bi_{0.76}Y_{0.22}Nb_{0.02}O_{1.5+\delta}$	975 °C/2 h	Cubic
	$x = 0.04$	$Bi_{0.76}Y_{0.20}Nb_{0.04}O_{1.5+\delta}$	975 °C/2 h	Cubic
	$x = 0.06$	$Bi_{0.76}Y_{0.18}Nb_{0.06}O_{1.5+\delta}$	975 °C/2 h	Cubic
	$x = 0.08$	$Bi_{0.76}Y_{0.16}Nb_{0.08}O_{1.5+\delta}$	975 °C/2 h	Cubic
	$x = 0.10$	$Bi_{0.76}Y_{0.14}Nb_{0.10}O_{1.5+\delta}$	975 °C/2 h	Cubic
$Bi_{0.76}Y_{0.24-x}Sc_xO_{1.5}$	$x = 0.02$	$Bi_{0.76}Y_{0.22}Sc_{0.02}O_{1.5}$	950 °C/2 h	Cubic
	$x = 0.04$	$Bi_{0.76}Y_{0.20}Sc_{0.04}O_{1.5}$	950 °C/2 h	Cubic
	$x = 0.06$	$Bi_{0.76}Y_{0.18}Sc_{0.06}O_{1.5}$	950 °C/2 h	Cubic
	$x = 0.08$	$Bi_{0.76}Y_{0.16}Sc_{0.08}O_{1.5}$	950 °C/2 h	Cubic
	$x = 0.10$	$Bi_{0.76}Y_{0.14}Sc_{0.10}O_{1.5}$	950 °C/2 h	Cubic
$Bi_{0.76}Y_{0.24-x}Zr_xO_{1.5+\delta}$	$x = 0.02$	$Bi_{0.76}Y_{0.22}Zr_{0.02}O_{1.5+\delta}$	950 °C/2 h	Cubic
	$x = 0.04$	$Bi_{0.76}Y_{0.20}Zr_{0.04}O_{1.5+\delta}$	950 °C/2 h	Cubic
	$x = 0.06$	$Bi_{0.76}Y_{0.18}Zr_{0.06}O_{1.5+\delta}$	950 °C/2 h	Cubic + rhombohedral
	$x = 0.08$	$Bi_{0.76}Y_{0.16}Zr_{0.08}O_{1.5+\delta}$	950 °C/2 h	Cubic + rhombohedral
	$x = 0.10$	$Bi_{0.76}Y_{0.14}Zr_{0.10}O_{1.5+\delta}$	950 °C/2 h	Cubic + rhombohedral
$Bi_{0.76}Y_{0.24-x}Ba_xO_{1.5-\delta}$	$x = 0.02$	$Bi_{0.76}Y_{0.22}Ba_{0.02}O_{1.5-\delta}$	825 °C/2 h	Cubic + rhombohedral
	$x = 0.04$	$Bi_{0.76}Y_{0.20}Ba_{0.04}O_{1.5-\delta}$	825 °C/2 h	Rhombohedral + unknown
	$x = 0.06$	$Bi_{0.76}Y_{0.18}Ba_{0.06}O_{1.5-\delta}$	825 °C/2 h	Rhombohedral + unknown
	$x = 0.08$	$Bi_{0.76}Y_{0.16}Ba_{0.08}O_{1.5-\delta}$	825 °C/2 h	Rhombohedral + unknown
	$x = 0.10$	$Bi_{0.76}Y_{0.14}Ba_{0.10}O_{1.5-\delta}$	825 °C/2 h	Rhombohedral + unknown

consequently increased the lattice constant. Berezovsky et al. also observed the existence of a second phase in their study examining the $(Bi_2O_3)_{0.71}(Y_2O_3)_{0.24}(ZrO_2)_{0.05}$ composition [35], though exact composition of the second phase was not specified. In the case of the $Bi_{0.76}Y_{0.24-x}Ba_xO_{1.5-\delta}$ ceramics, the XRD patterns shown in Fig. 1(f) reveal a major cubic phase and a minor rhombohedral phase whose intensity rose with the increase in the content of the BaO dopant. This observation is expected due to the fact that the highly conductive rhombohedral phase is generally obtained when Bi_2O_3 is doped with Sr, Ba, La, and other divalent or trivalent cations with a relatively large radius [10]. The peaks in the XRD patterns corresponding to the cubic phase shifted to higher 2θ values and those referred to the rhombohedral phase moved to lower 2θ values as the x value increased. Based on the facts that Ba^{2+} (1.42 Å) is much larger and Y^{3+} (1.02 Å) smaller than Bi^{3+} (1.17 Å), it can be concluded that the rhombohedral phase is rich in Ba^{2+} content and the Y^{3+} concentration in the cubic phase rises with the x value as Bi^{3+} is consumed by the formation of the rhombohedral phase. The calculated lattice parameters of the major cubic phase in the $Bi_{0.76}Y_{0.22}Ba_{0.02}O_{1.5-\delta}$, $Bi_{0.76}Y_{0.18}Ba_{0.06}O_{1.5-\delta}$ and $Bi_{0.76}Y_{0.14}Ba_{10}O_{1.5-\delta}$ ceramics appeared to be 5.5028 Å, 5.4957 Å, and 5.4886 Å, respectively, which confirmed the phase development in the $Bi_{0.76}Y_{0.24-x}Ba_xO_{1.5-\delta}$ ceramics.

Fig. 3 shows the typical SEM micrographs of the transgrainular fracture surfaces of the $Bi_{0.76}Y_{0.24-x}M_xO_{1.5}$ ceramics with maximum densification as compared to that of the $Bi_{0.76}Y_{0.24}O_{1.5}$ ceramic. The results indicated that all the ceramics were marked with a dense structure with little porosity. With the exception of the $Bi_{0.76}Y_{0.18}Ba_{0.06}O_{1.5-\delta}$ ceramic, all the ceramics appeared to have an analogous microstructure dotted with closed pores (<2 μm) and grain sizes ranging approximately from 5 to 10 μm. More specifically, the pores in the $Bi_{0.76}Y_{0.24-x}Zr_{x1.5+\delta}O_{1.5+\delta}$ system tended to coalense as the ZrO_2 dopant increased and some pores emerged to reach 10 μm in size. For the $Bi_{0.76}Y_{0.24-x}Ba_xO_{1.5-\delta}$ ceramics, the microstructure changed from granular to lamellar grains as the content of BaO dopant increased to 0.06 and beyond.

Fig. 4 presents the Arrhenius plot of the electrical conductivities of the $Bi_{0.76}Y_{0.24-x}M_xO_{1.5}$ ceramics with maximum densification compared to those of the $Bi_{0.76}Y_{0.24}O_{1.5}$ ceramic for reference. The electrical conductivities of $Bi_{0.76}Y_{0.24-x}Gd_xO_{1.5}$ at different temperatures, as shown in Fig. 4(b), increased with the rise in temperature. Similar to those reported in the literature, there was a slight bend at approximately 625 °C, due to the change in conductivity slopes resulted from a short-range order-disorder transformation in the oxygen sublattice [10,27,35]. For the $Bi_{0.76}Y_{0.24-x}Gd_xO_{1.5}$ compositions, no significant difference was observed in their electrical conductivities which were fairly close to those of the $Bi_{0.76}Y_{0.24}O_{1.5}$ ceramic, except for $Bi_{0.76}Y_{0.14}Gd_{0.10}O_{1.5}$ that revealed higher values of 0.13 and 0.30 Scm^{-1} respectively at 600 and 700 °C, much better than those of single-dopant added δ-Bi_2O_3 ceramics, such as the $Bi_{0.75}Y_{0.25}O_{1.5}$ and $Bi_{0.65}Gd_{0.35}O_{1.5}$ ceramics, as reported in the literature [8].

As revealed by Fig. 4(c), the electrical conductivity of the $Bi_{0.76}Y_{0.24-x}Nb_xO_{1.5}$ ceramics kept increasing with the rise in temperature. A clear bend in the conductivity slopes at approximately 625 °C was also observed, similar to the one observed by Berezovsky et al. [35]. Of the compositions with various Nb^{5+} contents, $Bi_{0.76}Y_{0.20}Nb_{0.04}O_{1.5+\delta}$ obtained the highest conductivities of 0.09 and 0.29 Scm^{-1} at 600 and 700 °C respectively, which are much higher than those in the δ-Bi_2O_3 systems with a single dopant of Y^{3+} or Nb^{5+} such as the $Bi_{0.75}Y_{0.25}O_{1.5}$ and $Bi_{0.75}Nb_{0.25}O_{1.5}$ ceramics as reported in the literature [8,27,36]. The conductivity of the $Bi_{0.76}Y_{0.24-x}Nb_xO_{1.5}$ ceramics showed a tendency of decreasing with increasing Nb^{5+} concentration due to the fact that the incorporation of Nb_2O_5 in the Bi_2O_3 lattice diminished the oxygen vacancies according to the following equation [36]:

$$Nb_2O_5 + 2V_O^{\cdot\cdot} \xrightarrow{Bi_2O_3} 2Nb_{Bi}^{\cdot\cdot} + 5O_O^{\times}$$

Though the conductivity of the Nb_2O_5-stabilized Bi_2O_3 was less than one-fifth of the conductivity of the Y_2O_3-stabilized Bi_2O_3 in the literature [36], the electric conductivities of the $Bi_{0.76}Y_{0.24-x}Nb_xO_{1.5}$

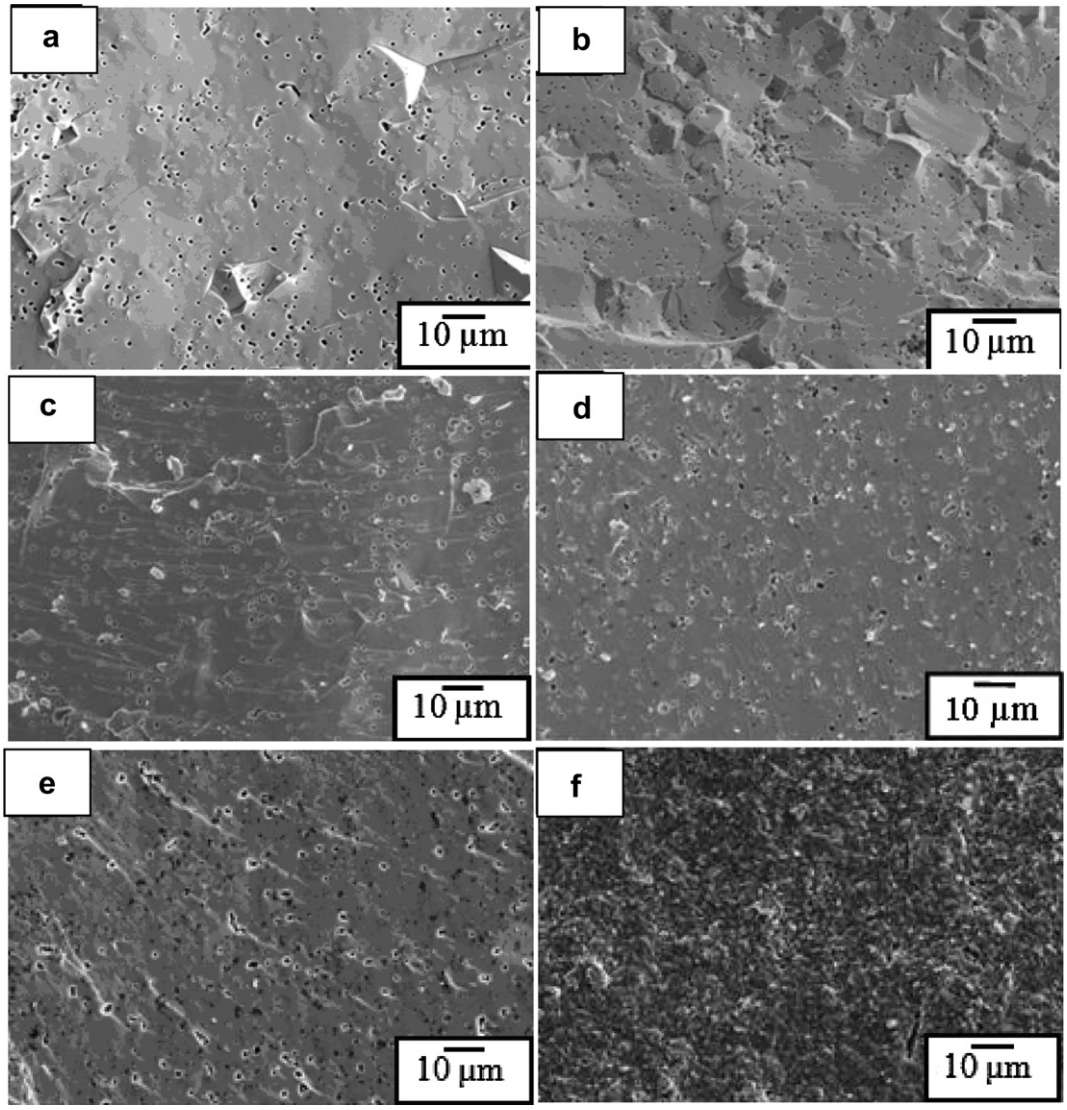

Fig. 3. SEM micrographs of fracture surfaces of (a) $Bi_{0.76}Y_{0.24}O_{1.5}$ ceramic (1025 °C/2 h), (b) $Bi_{0.76}Y_{0.14}Gd_{0.10}O_{1.5}$ ceramic (950°C/2 h), (c) $Bi_{0.76}Y_{0.20}Nb_{0.04}O_{1.5+\delta}$ ceramic (975 °C/2 h), (d) $Bi_{0.76}Y_{0.14}Sc_{0.10}O_{1.5}$ ceramic (950 °C/2 h), (e) $Bi_{0.76}Y_{0.16}Zr_{0.08}O_{1.5+\delta}$ ceramic (950 °C/2 h), and (f) $Bi_{0.76}Y_{0.18}Ba_{0.06}O_{1.5-\delta}$ ceramic (825 °C/2 h).

ceramics stabilized by co-dopants displayed no sign of being significantly inferior to those of other systems in the present study.

According to Fig. 4(d), the electrical conductivity of the Y_2O_3 and Sc_2O_3 co-doped Bi_2O_3 ceramics escalated with the increase in temperature and in the Sc^{3+} content of the $Bi_{0.76}Y_{0.24-x}Sc_xO_{1.5}$ ceramics. It should be noted that the bend induced by the change in the conductivity slopes and observed in previous two systems was not evident in this system. Enhancement in the electrical conductivity of the $Bi_{0.76}Y_{0.24-x}Sc_xO_{1.5}$ ceramics with Sc^{3+} content might be attributed to the improved densification of the ceramics with increasing Sc^{3+}, the relatively small ionic radius of Sc^{3+}, and the inability of isovalent substitution to diminish oxygen vacancy. The best composition, $Bi_{0.76}Y_{0.14}Sc_{0.10}O_{1.5}$, showed electrical conductivities of 0.20 and 0.46 Scm^{-1} respectively at 600 and 700 °C.

Fig. 4(e) shows the electrical conductivities of various $Bi_{0.76}Y_{0.24-x}Zr_xO_{1.5+\delta}$ ceramics at different temperatures which reveal different temperature-dependent behaviors determined by the Zr^{4+} content. While the electrical conductivity continued to increase with temperature, there was a clear bend at 600 °C of the conductivity-curve for the $Bi_{0.76}Y_{0.22}Zr_{0.02}O_{1.5+\delta}$ ceramic, similar to the previous case. Also observed was a drop in the conductivity of the $Bi_{0.76}Y_{0.14}Zr_{0.10}O_{1.5+\delta}$ ceramic at 575°C, which might be caused by the decomposition of the metastable δ-Bi_2O_3 into two isostructural fcc phases, two bcc phases isostructural to γ-Bi_2O_3, and traces of ZrO_2 as reported by Yaremchenko et al. in their study on the $(Bi_{0.95}Zr_{0.05})_{0.85}Y_{0.15}O_{1.5+\delta}$ system [29], though no electrical conductivity was given. A similar anomaly of sudden drop in electrical conductivity was further observed in the $(Bi_2O_3)_{0.75}(Tb_2O_3)_{0.25}$ ceramics at 600°C though they may not share a common mechanism [34]. It is apparent that δ-Bi_2O_3 retained its good conductivity in this system, in spite of the presence of the $Zr_{0.82}Y_{0.25}O_{1.91}O_{1.5+\delta}$ second phase and the lower oxygen-vacancy concentration resulted from the substitution of Zr^{4+} ions in the Bi_2O_3 lattice based on the following equation:

$$2ZrO_2 + V_O^{\cdot\cdot} \xrightarrow{Bi_2O_3} 2Zr_{Bi}^{\cdot} + 4O_O^{\times}$$

Of the $Bi_{0.76}Y_{0.24-x}Zr_xO_{1.5+\delta}$ ceramics studied, the $Bi_{0.76}Y_{0.20}Zr_{0.04}O_{1.5+\delta}$ ceramic emerged to sustain the best electrical conductivities of 0.27 and 0.55 Scm^{-1} at 600 and 700 °C respectively, significantly higher than those of the Y_2O_3-doped and the ZrO_2-dope3d Bi_2O_3 ceramics [10].

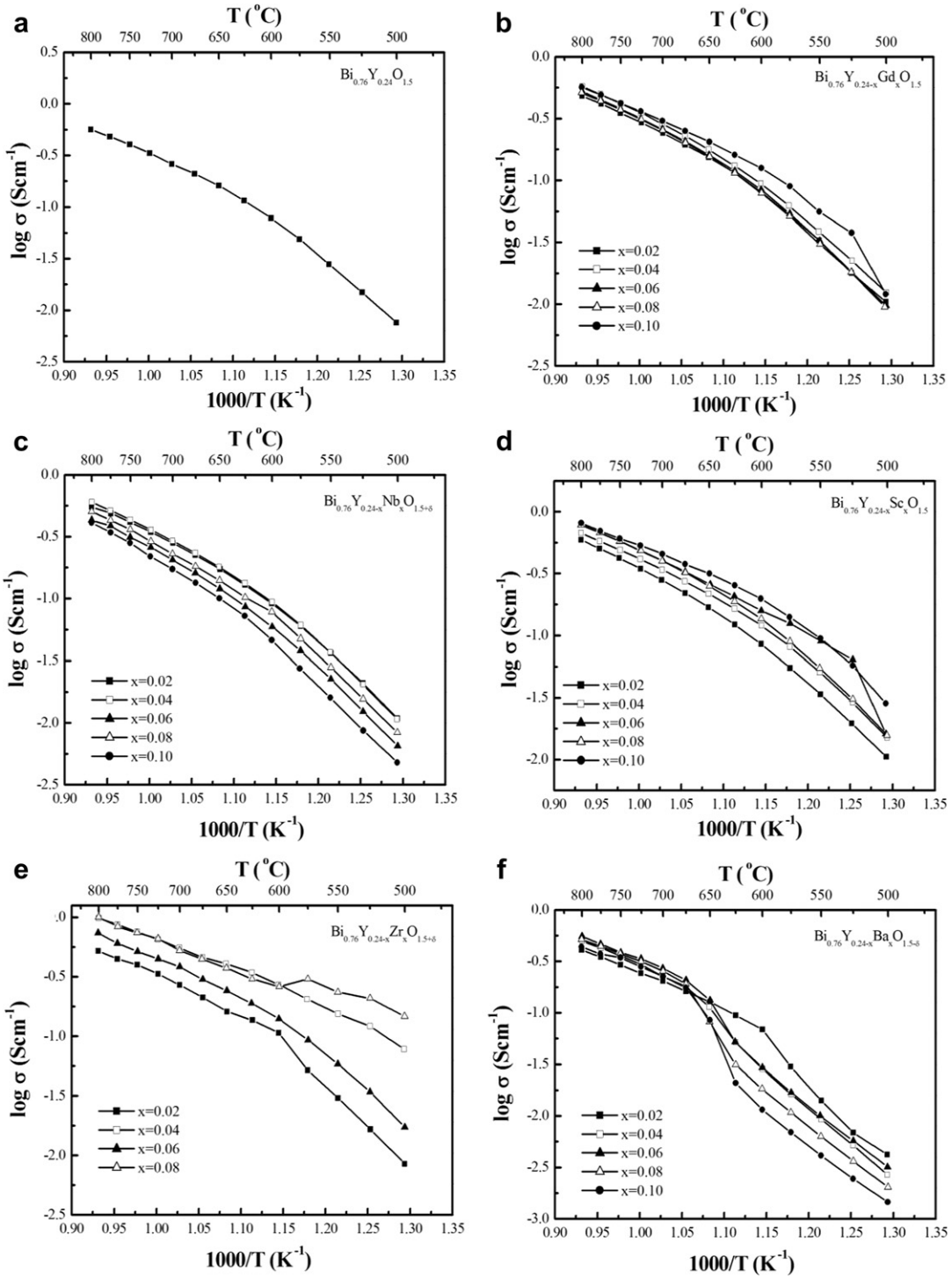

Fig. 4. Arrhenius plots of the electrical conductivities of (a) $Bi_{0.76}Y_{0.24}O_{1.5}$ ceramic (1025 °C/2 h), (b) $Bi_{0.76}Y_{0.24-x}Gd_xO_{1.5}$ ceramics (950 °C/2 h), (c) $Bi_{0.76}Y_{0.24-x}Nb_xO_{1.5+\delta}$ ceramics (975 °C/2 h), (d) $Bi_{0.76}Y_{0.24-x}Sc_xO_{1.5}$ ceramics (950 °C/2 h), (e) $Bi_{0.76}Y_{0.24-x}Zr_xO_{1.5+\delta}$ ceramics (950 °C/2 h), and (f) $Bi_{0.76}Y_{0.24-x}Ba_xO_{1.5-\delta}$ ceramics (825 °C/2 h).

As Fig. 4(f) indicates, the conductivity of the $Bi_{0.76}Y_{0.24-x}Ba_xO_{1.5-\delta}$ ceramics escalated with the rise in temperature. A bend in the conductivity curve at 600 °C with $x = 0.02$ and a sharp change in conductivity at approximately 650 °C with $x \geq 0.04$ were observed. The jump at 600–650 °C, a common feature of the BaO-, SrO-, CaO-doped Bi_2O_3, was regarded as a small configuration change in the relative position of atoms (β_1 to β_2 transition) within the rhombohedral crystal lattice that has also been observed in other systems [7,10,37,38]. The magnitude of the change increased with the Ba^{2+} content (i.e. x value) in the $Bi_{0.76}Y_{0.24-x}Ba_xO_{1.5-\delta}$ ceramics as the dopant triggered the formation of a rhombohedral phase. The conductivity decreased with the x value below the transition temperature and increased above the transition temperature. The best conductivity was observed in the $Bi_{0.76}Y_{0.18}Ba_{0.06}O_{1.5-\delta}$ composition and reached 0.03 and 0.27 S cm^{-1} respectively at 600 and 700 °C, much lower than those of the BaO-doped Bi_2O_3 and

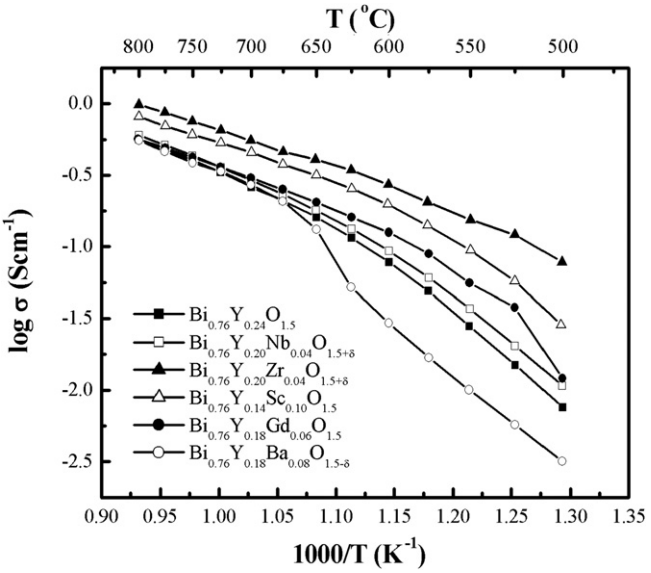

Fig. 5. Comparison of electrical conductivities of various $Bi_{0.76}Y_{0.24-x}M_xO_{1.5+\delta}$ ceramics, including $Bi_{0.76}Y_{0.24}O_{1.5}$ (1025 °C/2 h), $Bi_{0.76}Y_{0.14}Gd_{0.10}O_{1.5}$ (950 °C/2 h), $Bi_{0.76}Y_{0.20}Nb_{0.04}O_{1.5+\delta}$ (975 °C/2 h), $Bi_{0.76}Y_{0.14}Sc_{0.10}O_{1.5}$ (950 °C/2 h), $Bi_{0.76}Y_{0.16}Zr_{0.08}O_{1.5+\delta}$ (950 °C/2 h), and $Bi_{0.76}Y_{0.18}Ba_{0.06}O_{1.5-\delta}$ (825 °C/2 h).

Y_2O_3-doped Bi_2O_3 ceramics [8]. The substitution of Ba^{2+} in the Bi_2O_3 lattice seemed to facilitate no ion movement though the following equation indicates a rise in the concentration of oxygen vacancy.

$$2BaO \xrightarrow{Bi_2O_3} 2Ba'_{Bi} + 2O^{\times}_{O} + V^{\cdot\cdot}_{O}$$

According to Fig. 5 that compares the highest electrical performance of various systems and that of the $Bi_{0.75}Y_{0.25}O_{1.5}$ ceramic, $Bi_{0.76}Y_{0.20}Zr_{0.04}O_{1.5-\delta}$ emerged to be the best composition and $Bi_{0.76}Y_{0.14}Sc_{0.10}O_{1.5}$ the second, followed respectively by the $Bi_{0.76}Y_{0.14}Gd_{0.10}O_{1.5}$, $Bi_{0.76}Y_{0.20}Nb_{0.04}O_{1.5+\delta}$, and $Bi_{0.76}Y_{0.18}Ba_{0.06}O_{1.5-\delta}$ systems with their conductivities reaching similar values as the temperature increased; the difference in conductivity grew insignificant above 700 °C. The exception of $Bi_{0.76}Y_{0.18}Ba_{0.06}O_{1.5-\delta}$ may be due to the existence of dual (cubic and rhobohedral) phases and the smaller lattice constants. The conductivity of the $Bi_{0.76}Y_{0.24-x}M_xO_{1.5}$ ceramics seemed to show no strong correlation to the change in the concentration of oxygen vacancy resulted from the addition of co-dopants. It is reported in the literature that co-doping allows a much lower dopant concentration to stabilize the fcc phase at room temperature and subsequently leads to a higher conductivity based on the fact that conductivity increases linearly as total dopant concentration decreases with a fixed dopant ratio [8,18,26]. On the other hand, with the same total dopant concentration maintained by the present study, all systems, except for the $Bi_{0.76}Y_{0.18}Ba_{0.06}O_{1.5-\delta}$ ceramic, emerged to be superior to the $Bi_{0.75}Y_{0.25}O_{1.5}$ ceramic in terms of electrical conductivity. The result not only testifies to the ability of the co-dopant stabilized δ-Bi_2O_3 to improve electrical conductivity but also suggests that the nature of the co-doped ions also plays an important role in affecting conductivity. One of the reasons may be that the lattice constants of the co-dopant stabilized Bi_2O_3 ceramics are larger than those of their single-dopant stabilized counterparts.

4. Conclusions

Results of the study indicate that, compared to the $Bi_{0.76}Y_{0.24}O_{1.5}$ ceramic, the $Bi_{0.76}Y_{0.24-x}Gd_xO_{1.5}$, $Bi_{0.76}Y_{0.24-x}Nb_xO_{1.5+\delta}$, $Bi_{0.76}Y_{0.24-x}Sc_xO_{1.5}$, $Bi_{0.76}Y_{0.24-x}Zr_xO_{1.5+\delta}$, and $Bi_{0.76}Y_{0.24-x}Ba_xO_{1.5-\delta}$ ceramics revealed a lower sintering temperature. With the only exception of the $Bi_{0.76}Y_{0.24-x}Ba_xO_{1.5-\delta}$ ceramic, a cubic fluorite structure of δ-Bi_2O_3 phase was observed regardless of the x values. All the studied ceramics were marked with a dense structure with little porosity. Of the systems evaluated, $Bi_{0.76}Y_{0.20}Zr_{0.04}O_{1.5+\delta}$ demonstrated the best composition, followed by $Bi_{0.76}Y_{0.14}Sc_{0.10}O_{1.5}$. The conductivity of the $Bi_{0.76}Y_{0.24-x}M_xO_{1.5}$ ceramic seemed to register no strong correlation to the change in the concentration of oxygen vacancy caused by the addition of co-dopants. The δ-Bi_2O_3 stabilized by co-doping improved the electrical conductivity as compared to the one stabilized by single doping, probably due to the larger lattice constants.

References

[1] J.W. Fergus, J. Power Sources 162 (2006) 30–40.
[2] A.R. Ruffa, J. Mater. Sci. 15 (1980) 2258–2267.
[3] A.R. Ruffa, J. Mater. Sci. 15 (1980) 2268–2274.
[4] T.L. Wen, D. Wang, M. Chen, H. Tu, Z. Lu, Z.R. Zhang, H. Nie, Solid State Ionics 148 (2002) 513–519.
[5] E. Ivers-Tiffée, A. Weber, D. Herbstritt, J. Eur. Ceram. Soc. 21 (2001) 1805–1811.
[6] G. Zhong, J. Wang, Z. Zeng, Phys. Stat. Sol. (B) 245 (2008) 2737–2742.
[7] N.M. Sammes, G.A. Tompsett, F. .Aldinger, J. Eur. Ceram. Soc. 19 (1999) 1801–1826.
[8] P. Shuk, H.D. Wiemhofer, U. Guth, W. Gopel, M. Greenblatt, Solid State Ionics 89 (1996) 179–196.
[9] H.A. Harwig, A.G. Gerards, J. Solid State Chem. 26 (1978) 265–274.
[10] T. Takahashi, H. Iwahara, Mater. Res. Bull. 13 (1978) 1447–1453.
[11] Fuel Cell Handbook. seventh ed., EG&G Technical Services, Inc., USDOE, pp. 7–18.
[12] A. Laarif, F. Theobald, Solid State Ionics 21 (1986) 183–193.
[13] Q. Zhen, G.M. Kale, G. Shi, R. Li, W. He, J. Liu, Solid State Ionics 176 (2005) 2727–2733.
[14] T.N. Soitah, C. Yan, Curr. Appl. Phys. 10 (2010) 724–728.
[15] V. Fruth, A. Ianculescu, D. Berger, S. Preda, G. Voicu, E. Tenea, M. Popa, J. Eur. Ceram. Soc. 26 (2006) 3011–3016.
[16] C.K. Lee, A.R. West, Solid State Ionics 86–88 (1996) 235–239.
[17] S. Yilmaz, O. Turkoglu, I. Belenli, Mater. Chem. Phys. 112 (2008) 472–477.
[18] M.J. Verkerk, A.J. Burggraaf, J. Electrochem. Soc. 128 (1981) 75–82.
[19] M.J. Verkerk, A.J. Burggraaf, Solid State Ionics 3-4 (1981) 463–467.
[20] M.J. Verkerk, K. Keizer, A.J. Burggraaf, J. Appl. Electrochem. 10 (1980) 81–90.
[21] H. Kruidhof, K.J. De Vries, A.J. Burggraff, Solid State Ionics 37 (1990) 213–215.
[22] A.A. Yaremchenko, V.V. Kharton, E.N. Naumovich, A.A. Vecher, J. Solid State Electrochem. 2 (1998) 146–149.
[23] T. Takahashi, H. Iwahara, T. Esaka, J. Electrochem. Soc. 124 (1977) 1563–1569.
[24] G. Singla, P.K. Jha, J.K. r Gill, K. Singh, Ceram. Int. (2011).
[25] T. Esaka, T. Mangahara, H. Iwahara, Solid State Ionics 36 (1989) 129–132.
[26] D.W. Jung, K.L. Duncan, E.D. Wachsman, Acta Mater. 58 (2010) 355–363.
[27] G. Meng, C. Chen, X. Han, P. Yang, D. Peng, Solid State Ionics 28–30 (1988) 533–538.
[28] D. Mercurio, M.E. Farissi, B. Frit, Solid State Ionics 39 (1990) 297–304.
[29] A.A. Yaremchenko, V.V. Kharton, E.N. Naumovich, A.A. Tonoyan, Mater. Res. Bull. 35 (2000) 515–520.
[30] C.Y. Hsieh, H.S. Wang, K.Z. Fung, J. Eur. Ceram. Soc. 31 (2011) 3073–3079.
[31] S. Arasteh, A. maghsoudipour, M. Alizadeh, A. Nemati, Ceram. Int. 37 (2011) 3451–3455.
[32] T. Chou, L.D. Liu, W.C.J. Wei, J. Eur. Ceram. Soc. 31 (2011) 3087–3094.
[33] A. Watanabe, Solid State Ionics 86–88 (1996) 1427–1430.
[34] H.T. Cahen, T.G.M. Van Den Belt, J.H.W. de Wit, G.H.J. Broers, Solid State Ionics 1 (1980) 411–423.
[35] J. Berezovsky, H.K. Liu, S.X. Dou, Solid State Ionics 66 (1993) 201–206.
[36] A.V. Joshi, S. Kulkarni, J. Nachlas, J. Diamond, N. Weber, A.V. Virkar, J. Mater. Sci. 25 (1990) 1237–1245.
[37] T. Suzuki, T. Yamazaki, K. Kaku, M. Ikegami, Solid State Ionics 15 (1985) 241–2146.
[38] T. Suzuki, Y. Dansui, T. Shirai, C. Tsubaki, J. Mater. Sci. 20 (1985) 3125–3130.